JBC Papers in Press. Published on June 26, 2017 as Manuscript M117.780007
The latest version is at http://www.jbc.org/cgi/doi/10.1074/jbc.M117.780007

Interaction between the PH and START domains of ceramide transfer protein competes with phosphatidylinositol 4-phosphate binding by the PH domain

Jennifer Prashek[1], Samuel Bouyain[1], Mingui Fu[2], Yong Li[2], Dusan Berkes[3], and Xiaolan Yao[1]*

[1]Division of Molecular Biology and Biochemistry, School of Biological Sciences, University of Missouri-Kansas City, Kansas City, MO, 64110 United States
[2]Deparment of Basic Medical Science, School of Medicine, University of Missouri-Kansas City, Kansas City, MO, 64108 United States
[3] Department of Organic Chemistry, Slovak University of Technology in Bratislava, Radlinského 9, 81237 Bratislava, Slovakia

*Corresponding author**:** yaoxia@umkc.edu

Keywords: Ceramide transfer protein (CERT), lipid transport, sphingolipid, phosphatidylinositol, ceramide, X-ray crystallography, isothermal titration calorimetry (ITC), AlphaScreen, fluorescence resonance energy transfer (FRET)

ABSTRACT

De novo synthesis of the sphingolipid sphingomyelin requires non-vesicular transport of ceramide from the endoplasmic reticulum to the Golgi by the multidomain protein ceramide transfer protein (CERT). CERT's N-terminal pleckstrin homology (PH) domain targets it to the Golgi by binding to phosphatidylinositol 4-phosphate (PtdIns(4)P) in the Golgi membrane, while its C-terminal StAR-related lipid transfer domain (START) carries out ceramide transfer. Hyper-phosphorylation of a serine rich (SR) motif immediately following the PH domain decreases both PtdIns(4)P binding and ceramide transfer by CERT. This down-regulation requires both the PH and START domains, suggesting a possible inhibitory interaction between the two domains. In this study, we show that isolated PH and START domains interact with each other. The crystal structure of a PH/START complex revealed that the START domain binds to the PH domain at the same site for PtdIns(4)P binding, suggesting that the START domain competes with PtdIns(4)P for association with the PH domain. We further report that mutations disrupting the PH/START interaction increase both PtdIns(4)P-binding affinity and ceramide transfer activity of a CERT-SR phosphorylation mimic. We also found that these mutations increase the Golgi localization of CERT inside the cell, consistent with enhanced PtdInsPI(4)P binding of the mutant. Collectively, our structural, biochemical, and cellular investigations provide important structural insight into the regulation of CERT function and localization.

INTRODUCTION

Sphingolipids are fundamental components of cellular and organelle membranes. Its members are also involved in the regulation of a variety of biological processes such as membrane biogenesis, cell growth, apoptosis, senescence, migration and inflammation (1,2). Ceramide, the central building block for the syntheses of more complex sphingolipids, is synthesized in the endoplasmic reticulum (ER) and converted to glucosylceramide (GlcCer) and sphingomyelin (SM) in the Golgi. While the ceramide pool for GlcCer synthesis is delivered through vesicular trafficking, most of the ceramide used for SM synthesis is transported to the Golgi in a non-vesicular manner by the ceramide transfer protein (CERT) (3-6). The loss of CERT function leads to impaired SM synthesis in the Golgi, indicating its critical role in sphingolipid metabolism (5).

CERT contains multiple domains and motifs (Fig. 1*A*). The amino-terminal ~100 residue pleckstrin homology (PH) domain is responsible for targeting CERT to the Golgi apparatus by specifically recognizing phosphatidylinositol-4-monophosphate (PtdIns(4)P) (7,8). Following the

PH domain is a serine and threonine rich sequence termed the serine rich (SR) motif. The ceramide transfer activity of CERT is carried out by the C-terminal ~ 240 residue steroidogenic acute regulatory protein (StAR)-related lipid transfer (START) domain. Between SR and the START domain is the middle region (MR). MR is not predicted to contain any globular domains but harbors a short FFAT (two phenylalanines in an acidic tract) motif that associates with an ER-resident type II membrane protein, VAMP-associated protein A (VAP-A) (9,10). This association is enhanced by phosphorylation of Ser^{315}, which is adjacent to the FFAT motif (11). On the other hand, hyperphosphorylation of SR by protein kinase D and casein kinase Iγ2 decreases the PtdIns(4)P binding and ceramide transfer activity of CERT (12-14). Under SR hyperphosphorylation, the inhibition of PtdIns(4)P binding by the PH domain requires the presence of the START domain and the inhibition of the START domain ceramide transfer activity requires the PH domain (12). These findings suggest the possibility of an auto-inhibitory interaction between the PH and START domains and prompted our investigations.

Our data show that isolated PH and START domains interact with a dissociation constant (K_D) of ~ 9.2 μM. We also determined the crystal structure of a protein complex formed by these two domains. The structure reveals that the START domain interacts with PH domain at its PtdIns(4)P binding site. Moreover, the β1/β2 loop of the PH domain, which interacts with the membrane interfacial region, is completely shielded by the START domain (7,8). Competition assays indicate the START domain competes with PH domain association with PtdIns(4)P-containing liposomes. Consistent with the structural finding, disruption of the PH/START interaction in a SR phosphorylation mimic CERT restores both PtdIns(4)P binding and ceramide transfer activity. Moreover, with these mutations, CERT also exhibited increased Golgi localization. Altogether, our structural, biochemical and cellular investigations revealed that START domain associates with the PH domain at the same site utilized for PH domain membrane binding and confers CERT functional regulation.

RESULTS

Structure of the CERT PH and START Domain Complex

Phosphorylation of the Ser/Thr residues of CERT SR leads to down-regulation of PtdIns(4)P binding by the PH domain and ceramide transfer by the START domain. This regulation is suggested to involve a direct interaction between the PH and START domains of CERT (12). To understand the structural basis of CERT functional regulation, we solved the crystal structure of a PH/START complex to 2.4 Å limiting resolution (Table 1). Electron density allowed for building of 97 residues of the 103-residue PH domain and 235 of the 239-residue START domain. The structure contains two potential interfaces between the PH and START domains. The lower energy assembly (EBI PISA server), which also makes the most biological sense, is shown in Fig. 1*B* (15). The overall structure of the PH domain in the complex is nearly identical to that of the free CERT PH structure (PDB code 4HHV) (7,8). The root mean square deviation (rmsd) of superposition across PH Cα atoms is <1 Å with the greatest differences found in the β1/β2 loop. The START domain structure in the complex is also similar to that of the free CERT START domain. The rmsd of superposition of START domain in the complex with the START domain alone structure (PDB code 2E3N) across Cα atoms is <1 Å (16-18) (Fig. S1).

In the complex structure, the β6'/β7' and β8'/β9' loops of START domain clamp onto the β1/β2 loop of the PH domain and buries an interface of 614 $Å^2$ (Fig. 1*B* and 1*C*). Notably, the β6'/β7' loop of the START domain occupies the cavity of the PH domain that is used for PtdIns(4)P binding. Moreover, the β1/β2 loop of the PH domain, which makes significant energetic contributions to CERT PH domain association with membranes, is completely sandwiched by the β6'/β7' and β8'/β9' loops of the START domain (7,8). The PtdIns(4)P-binding site and the β1/β2 loop of the PH domain are collectively referred as the "basic groove" due to a significant number of basic residues in that area (7). The electrostatic surface potential maps of the PH and START domains in the complex show the negatively charged β6'/β7' loop of the START domain fits snuggly into the "basic groove" of the PH domain (Fig. 1*D*). Comparison of the CERT PH/START complex structure with a HADDOCK generated structure

model of the PH/diC6-PtdIns(4)P complex shows a clash between START domain and diC6-PtdIns(4)P binding to PH domain (7,8,19) (Fig. 1*E*). These observations suggest that PH domain binding to START domain is incompatible with its association with PtdIns(4)P-containing membranes.

We also used nuclear magnetic resonance (NMR) chemical shift perturbation to examine the binding interface between the PH and START domains. Adding unlabeled START domain to ^{15}N-labeled PH domain leads to reduction or complete loss of the peak intensities of some residues, suggesting intermediate exchange in the PH domain in the presence of the START domain (Fig. S2*A*). The residues that vanished or showed 90% or more reduction of peak intensity are mapped onto the crystal structure of the PH domain (PDB code 4HHV) (Fig. S2*B*). As a comparison, shown in Fig. S2*C* are residues that are affected by the addition of diC6-PtdIns(4)P to ^{15}N labeled PH domain (8). It can be observed that perturbations of the PH domain by START domain and diC6-PtdIns(4)P occur in similar regions, indicating overlapping binding interfaces. The findings from these NMR studies is consistent with the PH/START complex crystal structure (Fig. 1*B*).

Details of the CERT PH/START Complex Interface

EBI PISA and CCP4 program CONTACT were used to analyze the PH/START interface (15,20) (Fig. 2*A*). The PH and START domain interface consists of 20 residues from PH and 17 residues from START. Specifically, Lys^{32}, Trp^{33}, Tyr^{36}, Trp^{40}, Arg^{43}, Tyr^{54}, Arg^{66}, and Tyr^{96} of the PH domain form multiple contacts with the START domain. These PH domain interface residues are also involved in binding to PtdIns(4)P-containing membranes, either through direct interactions with PtdIns(4)P or through interactions with the membrane interfacial region (7,8), i.e., the PH domain uses the same set of residues for START domain and PtdIns(4)P-containing membrane interaction. Three residues in the β6'/β7' loop of the START domain, Glu^{494}, Asn^{495}, and Glu^{498} form extensive hydrogen bonds with PH domain residues Lys^{32}, Tyr^{36}, Arg^{43}, Tyr^{54} and Arg^{66} (Fig. 2*B* and *2C*). Phe^{598}, the last residue of the START domain, interacts with Tyr^{36} through π-π stacking (Fig. 2*C*). Val^{533} and Pro^{535} in the β8'/β9' loop make hydrophobic contacts with PH domain residues Trp^{33}, Trp^{40} and Tyr^{96} (Fig. 2*D*). In addition, the backbone CO of Val^{533} forms a hydrogen bond with Trp^{33} indole ring NH group (Fig. 2*D*). The β8'/β9' loop of the START domain, though not in direct competition with the PH domain PtdIns(4)P binding site, shields the β1/β2 loop and would therefore prevent PH/membrane association. The PH/START complex structure clearly suggests that PtdIns(4)P and START domain binding by the PH domain are incompatible interactions.

CERT PH Domain Interacts with START Domain with Micro-molar Affinity

Isothermal titration calorimetry (ITC) was used to determine the affinity between the PH and START domains. ITC measurements were performed by injecting PH protein into START protein. Global fitting of three separate measurements using a single-site model yields a ΔH of -12.1 (-13.1, -11.3) kcal/mol and a K_D of 9.2 (8.1, 10.5) μM (Fig. 3).

To evaluate the contributions of interface residues in the interaction, site-directed mutants were generated in both the PH and START domains. The abilities of these mutants to compete for binding against the wild-type PH/START interaction were assessed in an AlphaScreen competition assay (21) (Fig. 4*A*). IC_{50} values of 2.0 and 2.2 μM were obtained for wild-type (WT) PH and START domains respectively (Fig. 4*B-D)*. A PH domain R43A mutant showed more than 8-fold increase in IC_{50} (16.8 μM) as compared with PH WT (Fig. 4*B* and *4D*). However, the IC_{50} for the Y54A mutant (1.5 μM) is similar to that of the PH WT and the IC_{50} values for the R43A/Y54A and the R43A mutants are also close to each other (Fig. 4*B* and *4D*). One-way ANOVA statistics indicate that the IC_{50} differences measured for the R43A and R43A/Y54A mutants versus PH WT domain were statistically significant, whereas Y54A was not (Fig. 4*E*). These results indicate that Arg^{43} significantly contributes to the PH/START interaction whereas the contribution from Tyr^{54} is negligible. It is likely that despite the short distance, Tyr^{54} is not positioned at an optimal orientation for hydrogen bond formation with Glu^{494}. It is also conceivable that other nearby basic residues, such as Lys^{56}, may engage in interactions with Glu^{494} in the Y54A mutant, thus making this residue less critical for START

domain binding. We also attempted to measure the IC_{50} of a W33A/R43A/Y54A PH domain mutant, but the experiments were unsuccessful. Using NMR ^{15}N-^{1}H 2D heteronuclear single-quantum correlation (HSQC) experiments we found that the W33A/R43A/Y54A mutant maintains the overall tertiary fold of the PH domain (Fig. S3). We speculate the difficulties with these experiments were likely caused by protein aggregation at high concentrations in the presence of the AlphaScreen beads. As an alternative to the AlphaScreen competition assay, we used 2D HSQC experiments to evaluate the effect of the W33A/R43A/Y54A mutations on START domain binding. The presence of 1x unlabeled PH WT domain lead to extensive broadening of the ^{15}N-labeled START domain peaks, likely from intermediate binding exchange (Fig. S4*A*). In contrast, the addition of 1x PH W33A/R43A/Y54A mutant lead to little change in the START domain spectrum, suggesting a much-reduced affinity between the PH W33A/R43A/Y54A mutant and the START domain (Fig. S4*B*).

To validate the role of the β6'/β7' and β8'/β9' loops of the START domain in the PH/START interaction, START domain mutants E494R/N495K, E494R/N495K/P535R/E537K, and a mutant in which a $(GGS)_2$ linker replaces the β6'/β7' loop (Δ493-498 $(GGS)_2$) were tested in the AlphaScreen competition assay (Fig. 4*A*). The E494R/N495K and the Δ493-498 $(GGS)_2$ mutants both displayed significant decreases in affinity compared to START WT domain with an IC_{50} of 34.7 and 59.5 μM respectively, demonstrating the importance of the β6'/β7' loop in mediating the PH/START interaction (Fig. 4*C-E*). The E494R/N495K/P535R/E537K mutant showed the most loss in affinity with an IC_{50} of 86.1 μM, confirming that both loops of the START domain contribute to PH domain binding (Fig. 4*C-E*). Altogether, these competition assays establish that the START domain uses the β6'/β7' and β8'/β9' loops to engage with the PtdIns(4)P binding site of the PH domain.

CERT PH/START Interaction is Incompatible with PH domain Binding to PtdIns(4)P

The crystal structure of the PH/START complex predicts that START domain competes with PtdIns(4)P-containing membranes for binding to the PH domain (7,8). To test this hypothesis, an AlphaScreen competition assay in which the ability of START domain to compete against PtdIns(4)P-embedded liposomes for PH domain association was evaluated (Fig. 5*A*). An IC_{50} value of 1.5 μM was obtained for the PH WT protein, which is comparable to the reported affinity of the PH domain for PtdIns(4)P-embedded liposomes (7,8). The START domain yielded an IC_{50} value of 4.4 μM, indicating that it is able to compete with the PH/liposome interaction (Fig. 5*B*). The START domain has been shown to interact with membranes weakly (16,18). To evaluate how START domain association with membrane affects the competition, the assays were repeated in the presence of a START domain inhibitor, (1R, 3S)-N-(3-Hydroxy-1-hydroxymethyl-3-phenylpropyl) dodecanamide (HPA-12), which has been shown to abolish START domain membrane binding (22-24). The presence of (1R, 3S)-HPA-12 slightly increased the IC_{50} of the START domain, but the difference was not significant (Fig. S5*A* and S5*B*), indicating START/PH interaction is likely responsible for the competition.

Disrupting the PH/START Interaction Restores CERT SR Phosphorylation Mimic PtdIns(4)P Binding and Ceramide Transfer Activity

Our investigations on isolated PH and START domains indicate PH/START binding competes with PH domain binding to PtdIns(4)P-containing membranes. To further investigate the role of this interaction in the regulation of full-length CERT, we made use of a SR phosphorylation mimic of CERT, termed CERT10E, where the Ser/Thr residues of SR are mutated to Glu residues (12). We generated a CERT10E E494R/N495K/P535R/E537K mutant and investigated the effects of disrupting the PH/START interaction on CERT10E PtdIns(4)P binding and ceramide transfer activity.

FRET between protein Trp residues and Dansyl-PE lipids embedded in liposomes was used to assess the binding of proteins to the liposomes (25). In the absence of PtdIns(4)P, neither CERT10E nor the CERT10E E494R/N495K/P535R/E537K mutant exhibits any detectable FRET, indicating absence of association with the liposomes (Fig. 6*A*). In the presence of 4mol% PtdIns(4)P in the liposomes, low FRET

was detected between the CERT10E and liposomes, suggesting weak association. This is consistent with previous studies demonstrating that phosphorylated CERT has low affinity for PtdIns(4)P-embedded membranes (12-14). The CERT10E E494R/N495K/P535R/E537K mutant showed a clear increase in FRET signal as compared to CERT10E, indicating increased affinity for PtdIns(4)P-containing liposomes in the absence of the PH/START interaction. The data shown in Fig. 6*A* are performed with 40 μM total liposome concentration. The binding experiments were also carried out with 60 and 80 μM liposomes and similar increases in PtdIns(4)P binding of CERT10E E494R/N495K/P535R/E537K compared to CERT10E were observed (Fig. S6*A-B*). This result was also consistent with prior work showing that the affinity of CERT10E for PtdIns(4)P increased following cleavage of either the PH or START domain (12).

To investigate if the PH/START complex interface revealed in this study is involved in the phosphorylation inhibition of CERT ceramide transfer activity, the activities of CERT10E and the CERT10E E494R/N495K/P535R/E537K mutant were compared. The transfer activity assay utilized two types of liposomes: donor liposomes that contained AV-Cer, a fluorescent ceramide analogue, and its quencher, DiO-C_{16}, and acceptor liposomes that contain 4mol% PtdIns(4)P. Transfer of AV-Cer into acceptor liposomes that do not contain the quencher allowed for detection of AV-Cer emission (26,27). CERT10E, consistent with previous results, exhibits very low ceramide transfer activity (12) (Fig. 6*B* and Fig. S6*C*). In comparison, the CERT10E E494R/N495K/P535R/E537K showed much higher ceramide transfer activity than CERT10, despite the fact that the E494R/N495K/P535R/E537K mutations decreased the intrinsic ceramide transfer activity of the isolated START domain (Fig. 6*C* and Fig. S6*D*). These results indicate that the PH/START interface identified in our structural investigation is involved in SR phosphorylation regulation of CERT ceramide transfer activity. These results are also consistent with prior studies showing removal of PH domain leads to increase in the ceramide transfer activity of CERT10E (12). Ideally, mutations on the PH domain that disrupt PH/START binding but not the intrinsic ceramide transfer activity of the START domain should have been used here. However, such mutations on the PH domain would also impact PtdIns(4)P-binding by PH, so as a compromise the E494R/N495K/P535R/E537K mutant was used in these experiments.

While the PH/START complex crystal structure provides a clear explanation for the inhibition of PtdIns(4)P-binding by the START domain, it is not immediately clear how this interaction affects the ceramide transfer activity of the START domain. To address this question, the ceramide transfer activity of the isolated START domain in the presence of PH WT or PH W33A/R43A/Y54A mutant were compared. Due to the moderate affinity between isolated PH and START domains and the relatively low concentration of START domain used in the transfer assay, an excess amount of PH domain was used so that ~ 90% of the START domain would exist in the PH domain-bound form. The activity of the START domain in the presence of PH WT was decreased, though not significantly, compared to the activity in the presence of PH W33A/R43A/Y54A (Fig. S7*A, D* and *E*). However, the excess of both PH WT and mutant proteins caused unexpected changes to the activity of the START domain (Fig. S7*B*). Because non-vesicular lipid transfer mediated by lipid transfer proteins is a multi-step process that requires the transfer protein to adopt different conformations during lipid extraction, lipid transport, and lipid release, the high concentrations of protein in solution may have led to modulations of the conformational equilibrium of the START domain and its affinity for membranes, which could result in changes in the transfer activity. To determine if these changes to activity were the result of non-specific effects from the high concentrations of PH proteins used in this assay, the ceramide transfer activity of START domain was measured in the presence of excess B1 immunoglobulin-binding domain of streptococcal protein G (GB1), which does not interact with START domain and is not related to the PH domain (28-30) (Fig. S7*B* and *C*). Indeed, the presence of GB1 altered the rate for transfer in a manner nearly identical to PH W33A/R43A/Y54A protein, which also does not bind the START domain, indicating a non-specific effect on START activity (Fig. S7*D* and *E*). Altogether,

these results show that the START domain is not inhibited by binding to the isolated PH domain alone. Therefore, while the PH/START interaction does play a role in the phosphorylation inhibition of CERT ceramide transfer activity, the interaction is not directly responsible for inhibiting the START domain and additional factors are involved in the SR phosphorylation inhibition of CERT function.

Disrupting the PH/START Interaction Changes the Cellular Distribution of CERT

The FRET based liposome binding experiments show that disrupting the PH/START interaction increased PtdIns(4)P binding of the CERT SR phosphorylation mimic, CERT10E (Fig. 6*A*). Based on this result, one would predict that disrupting the PH/START interaction would increase the Golgi localization of CERT. To test this hypothesis, immunofluorescence microscopy was used to assess the role of the PH/START interaction in the cellular localization of CERT. HEK293 cells were transiently transfected with HA-tagged CERT or CERT E494R/N495K/P535R/E537K mutant. Using GM130 as a Golgi marker, the cells were visualized by indirect immunofluorescence with anti-HA and anti-GM130 antibodies (Fig. 7). HA-CERT exhibited even distribution in the perinuclear region, likely due to association with VAP-A in the ER membrane (5) (Fig. 7). In contrast, HA-CERT E494R/N495K/P535R/E537K showed clear preferential co-localization with GM130, indicating release of inhibition of CERT binding to the Golgi membrane. Interestingly, the cellular distribution of HA-CERT E494R/N495K/P535R/E537K is very similar to that of the CERT S132A mutant, where SR cannot be phosphorylated, suggesting HA-CERT E494R/N495K/P535R/E537K resembles the non-phosphorylated CERT (31). These similarities further illustrate that the PH/START interaction is responsible for SR phosphorylation inhibition of CERT association with the Golgi membrane. Our study provides a structural explanation for the previous observations that the inhibition of SR phosphorylated CERT binding to the Golgi membrane requires the START domain (12).

DISCUSSION

In this study, we showed that CERT PH domain interacts with the START domain through the PtdIns(4)P binding site of PH (7,8) (Fig. 1-4, Fig. S2). As a consequence, isolated START domain competes with PtdIns(4)P-embedded liposomes for PH domain association (Fig. 5). These findings on isolated PH and START domains were further investigated in a full-length CERT SR phosphorylation mimic, CERT10E, which has much reduced PtdIns(4)P binding affinity as well as low ceramide transfer activity (12). Introducing the E494R/N495K/P535R/E537K mutations, which abolish the PH/START interaction, into CERT10E leads to recovery of both PtdIns(4)P binding and ceramide transfer activity of CERT10E (Fig. 6). We also used immunofluorescence to compare the cellular localization of wild type CERT and a CERT E494R/N495K/P535R/E537K mutant. While the wild type CERT exhibits even distribution in the perinuclear region, the mutant CERT protein preferentially concentrates on the Golgi (Fig. 7).

The PH/START binding interface does not overlap with the ceramide-binding cavity of the START domain (Fig. S1). It is also distant from the two residues (Trp^{473} and Trp^{562}) shown to be critical for ceramide extraction and release (16,18) (Fig. S1). Not surprisingly, we found that in the context of isolated domains, PH domain binding has a negligible effect on START domain activity (Fig. S7). This finding implies that the inhibition of CERT transfer activity by SR phosphorylation is not a direct result of PH domain binding to the START domain. We speculate that there are additional factors involved in the phosphorylation inhibition of CERT function. Indeed, previous studies showed that the ceramide transfer activity of a CERT SR phosphorylation mimic increased with removal of the PH domain, but further removal of the middle region (MR) led to an even greater increase in ceramide transfer activity (5,7). Consistent with these previous results from other labs, we also observed that in our FRET-based ceramide transfer assays, the START domain alone is much more active than the full-length CERT proteins (Fig. 6*B*-*C* and Fig. S7). These observations suggest the possibility that MR is also involved in the suppression of START domain activity. Further investigations are needed to fully understand the structural basis of CERT functional regulation.

In summary, our combined structural, biochemical and cellular investigations establish that the CERT PH and START domain interaction competes with PH domain binding to PtdIns(4)P-containing membranes and plays an important role in the regulation of CERT cellular localization and ceramide transfer. Our findings provide structural insights into a previous study that show PH and START domains are required for SR phosphorylation inhibition of CERT binding to PtdIns(4)P and ceramide transfer (12). Our investigation also raises additional questions regarding the structural mechanism of START domain inhibition in CERT under SR hyperphosphorylation. We are currently investigating these questions.

Lastly, we would like to comment on a practical aspect of research on CERT protein based on our findings. In various investigations, it is often necessary to add either N- or C-terminal tags to the protein of interest for purification or detection purposes. Our studies here show that the very last residue of CERT, Phe^{598}, which belongs to the START domain, makes intimate contact with Tyr^{36} of the PH domain and contributes to PH/START interaction (Fig. 2A and 2C). As a result, a C-terminal tag in CERT could potentially interfere with PH/START binding and lead to experimental artifacts. To avoid this, the sequence of C-terminal tag on CERT needs to be carefully chosen.

EXPERIMENTAL PROCEDURES

Materials

Lipids were obtained from Avanti Polar Lipids unless otherwise specified. AlphaScreen technology materials and equipment were purchased from PerkinElmer Life Sciences. The primary rat monoclonal anti-HA antibody was purchased from Sigma-Aldrich. The primary mouse polyclonal antibody to GM130 and the secondary antibodies, anti-rat IgG labeled with Alexa Fluor® 488 and anti-mouse IgG labeled with Alexa Fluor® 594, were purchased from Abcam.

Protein Expression and Purification

The human CERT PH domain containing residues 20 to 122 and START domain containing residues 360 to 598 were cloned into the prokaryotic overexpression vector $pHis_6$-GB1 as previously described (8). DNA molecules encoding CERT PH domain with an N-terminal c-Myc epitope tag and START domain with a Cys residue added to the N-terminus were purchased from GenScript in the $pHis_6$-GB1 vector. Site-specific biotinylated START domain was produced using the EZ-Link Maleimide-PEG_2-Biotin reagent (Thermo Scientific) according to the manufacturer's instructions. Mass spectrometry confirmed single or double biotinylation of the START domain. The full-length, phosphorylation mimic CERT (CERT10E) was created by site-directed mutagenesis of wild-type human CERT (CERT) to mutate S132, S135, S138, S141, S144, T146, S147, T148, S149, and S150 to glutamate (Kumagai et al., 2007). CERT10E was cloned into the $pHis_6$-GB1 vector with six extra amino acids (GEFKGL) added at the N-terminus after cloning. All additional mutations were created by site-directed mutagenesis and individual clones were confirmed by DNA sequencing. Proteins were expressed and purified as previously described (8). The PH and START domain mutants were uniformly labeled with ^{15}N and 2D ^{15}N-^{1}H nuclear magnetic resonance (NMR) heteronuclear single-quantum correlation (HSQC) spectra show the mutants maintain the overall fold of the wild-type protein (data not shown).

Crystallization, X-ray Diffraction Data Collection, Structure Solution, and Refinement

Crystallization experiments were carried out by vapor diffusion of hanging drops. CERT PH/START co-crystals appeared in 5-7 days at 20 °C using 0.1 M MES bis-tris (pH 6.0), 6% (w/v) polyethylene glycol 10,000, and 10 μM calcium chloride. Individual drops consisted of 1 μl of PH/START complex sample (8 mg/ml) and 1 μl of precipitant solution. Crystals were cryoprotected by a brief incubation in precipitant solution containing 24% (w/v) polyethylene glycol 400. Crystal samples were preserved by flash-cooling in liquid nitrogen.

X-ray diffraction data were collected at -173 °C using beamline 22-BM of the Advanced Photon Source (Argonne National Laboratory). Individual reflections were indexed, integrated and scaled using HKL2000 (32). Initial phase information was obtained by maximum-likelihood molecular replacement using the program Phaser using available crystal structures of the PH (PDB code

4HHV) and START (PDB code 2E3M) domains (33,34). An initial model was built in PHENIX.AUTOBUILD. The final model was obtained after manual building in COOT followed by additional rounds of refinement using the refine program of Phenix (20,35-37). The model was analyzed and validated using MOLPROBITY before PDB deposition with the accession code 5JJD (38). Structure representations were generated using PyMOL (39). Additional structural information and refinement statistics are presented in Table 1.

Isothermal Titration Calorimetry

CERT PH and START domains were exchanged into buffer containing 25 mM Hepes (pH 7.5), 100 mM sodium chloride and 2 mM β-mercaptoethanol. All ITC experiments were carried out on a MicroCal VP-ITC instrument (Northhampton, MA). The first set of ITC data was collected by injecting 290 µl of 300 µM PH domain into 1.4 ml of 30 µM START domain with 10 µl injections. Later experiments were performed with 3 µl and 7 µl injections of 400 µM PH domain into 40 µM START domain. Protein solutions were held at 30 °C with a 290 rpm stirring speed and a 120 s delay between injections.

Each data set was first analyzed with the NITPIC program which determined the injection peak baselines, integrated the areas of injection heats, prepared an isotherm, and estimated the initial parameter values (40,41). Global fitting of all data sets was carried out using SEDPHAT 10.58d (42,43). ITC data plots were then prepared with GUSSI 1.0.8d (44).

AlphaScreen Competition Assay

Binding between CERT PH and START domains or PtdIns(4)P-embedded liposomes was evaluated using a luminescent microbead AlphaScreen technology (21). In this assay c-Myc PH domain was mixed with equimolar biotinylated START domain or biotinylated-PE and PtdIns(4)P-embedded liposomes and increasing concentrations of untagged competitor proteins. Acceptor beads coated with anti-c-Myc antibody and streptavidin coated donor beads were added to adsorb the c-Myc PH domain and biotinylated START domain or biotinylated-PE and PtdIns(4)P-embedded liposomes, respectively. Upon illumination at 680 nm a photosensitizer in the donor beads converts ambient oxygen to singlet oxygen. If the acceptor beads are within close proximity to the donor beads, energy is transferred from the singlet oxygen to thioxene derivatives on the acceptor bead, resulting in emission at 520-620 nm.

Using the AlphaScreen c-Myc detection kit from PerkinElmer Life Sciences, an equilibrium competition binding-assay was carried out in 96-well format ½ area opaque plates with the following procedures. Competition assays with CERT PH and START domains were carried out in a final reaction volume of 25 µl. Each component was added to the following final concentrations in buffer containing 25 mM Hepes (pH 7.5), 100 mM sodium chloride and 0.1% (w/v) BSA: 200 nM c-Myc PH domain, 200 nM biotinylated START domain, 20 µg/ml anti-c-Myc AlphaScreen acceptor beads and 20 µg/ml AlphaScreen Streptavidin donor beads. A dilution series of the untagged competitor protein was prepared with final concentrations ranging from 20 nM to 200 µM. The reaction began by mixing c-Myc PH domain, biotinylated START domain and varying concentrations of the unlabeled competitor. Following incubation for 1 h at room temperature, acceptor beads were added and incubated for 1 h. Donor beads were then added and after a 1 h incubation the AlphaScreen signal was read on an EnSpire multimode plate reader. Competition assays with c-Myc PH domain and biotinylated-PE and PtdIns(4)P-embedded liposomes were carried out with the same procedure but with a final concentration of 200 nM liposomes in place of biotinylated START domain. Liposomes containing 1,2-dioleoyl-sn-glycero-3-phosphocholine (DOPC), 1,2-dioleoyl-sn-glycero-3-phospho-L-serine (DOPS), porcine brain PtdIns(4)P, and 1,2-dioleoyl-sn-glycero-3-phosphoethanolamine-N-(cap biotinyl) (biotinyl-cap PE) were prepared at a molar ratio of 84.6/9.4/4/2 by the extrusion method using 0.1 µm pore size membranes (Avanti Polar Lipids).

The AlphaScreen signal was normalized to wells without competitor. A dose-response curve was generated by plotting normalized signal (%) versus log[competitor (M)]. IC_{50} values were calculated by nonlinear curve-fitting to a one-site competition model using GraphPad Prism7 software (GraphPad; La Jolla, CA). IC_{50} values are reported

as averages ± standard deviations from two or three experiments.

Fluorescence Resonance Energy Transfer Measurement of Protein-Liposome Interaction
Fluorescence resonance energy transfer (FRET) between Dansyl-PE (1,2-dioleoyl-sn-glycero-3-phosphoethanolamine-N-(5-dimethylamino-1-naphthalenesulfonyl) embedded in liposomes and Trp residues of CERT10E or CERT10E E494R/N495K/P535R/E537K protein was used to monitor the protein/liposome interaction. Liposomes that contain either DOPC/DOPS/Dansyl-PE/PtdIns(4)P at a molar ratio of 77.4/8.6/10/4 or DOPC/DOPS/Dansyl-PE at a molar ratio of 81/9/10 were prepared by the extrusion method using 0.1 μm pore size membranes. Liposomes were suspended in a total volume of 1.2 ml buffer containing 25 mM Tris (pH 7.5), 100 mM NaCl, 1 mM EDTA, and 1 mM TCEP. The buffer also contained 8.25 μM of the (1R, 3S)-N-(3-Hydroxy-1-hydroxymethyl-3-phenylpropyl) dodecanamide (HPA-12) to abolish START domain interaction with liposome (22-24). CERT10E or CERT10E E494R/N495K/P535R/E537K protein is added to the vesicle suspension under constant stirring at 25 °C. Trp residues were excited at 290 nm and Dansyl-PE emission was monitored at 400-550 nm. Emission intensity at 530 nm was chosen for FRET analyses to ensure absence of intensity contribution from the protein. The normalized FRET intensity (ΔF) at a given protein concentration was calculated with the following equation: $\Delta F = (F_i - F_0) / F_0$, where F_0 is the intensity in the absence of protein and F_i is the intensity after protein addition. The titration series were performed with liposome concentrations of 40, 60 and 80 μM. For each vesicle concentration, the normalized FERT values were plotted against protein concentration to compare the binding of CERT10E and CERT10E E494R/N495K/P535R/E537K to liposomes.

FRET Measurement of Ceramide Transfer Activity
The ceramide transfer activities of CERT10E and START proteins were measured using donor liposomes containing ceramide and acceptor liposomes that do not (26,27). The donor liposomes were prepared with DOPC, DOPS, 3,3'-dihexadecyloxacarbocyanine (DiO-C_{16}) (Genolite Biotek), N-octanoyl-D-erythro-sphingosine (C8-Cer), and a fluorescent ceramide analogue called anthrylvinyl-ceramide (AV-Cer) (Cayman Chemical) at a molar ratio of DOPC/DOPS/DiO-C_{16}/C8-Cer/AV-Cer (79.2/8.8/3/8/1) (27). The acceptor liposomes were composed of DOPC/DOPS/PtdIns(4)P at a molar ratio of 86.4/9.6/4.0. Liposomes were prepared by the extrusion method using 0.1 μm pore size membranes. AV-Cer emission is quenched by DiO-C_{16} in the donor liposomes but becomes detectable upon transfer to the acceptor liposomes. The ceramide transfer assays were performed in buffer containing 25 mM Tris (pH 7.5), 100 mM sodium chloride, 1 mM EDTA, and 1 mM TCEP with 1.4 ml total volume at 25 °C with constant stirring. The emission of AV-Cer at 420 nm was monitored following excitation at 370 nm. 6 μM donor and 60 μM acceptor liposomes were added first. After ~100 s, ceramide transfer was initiated by adding 80 nM protein. No spontaneous transfer was observed in the absence of protein addition. At the end of the assay, 3.5% (v/v) Triton X-100 was added to disrupt the liposomes and release all AV-Cer molecules to give the maximum fluorescence. Fluorescence intensities were corrected for background by subtracting the intensity before the initiation of ceramide transfer. The percent of AV-Cer transferred at each time point was calculated by dividing the corresponding intensity by the maximum intensity. Ceramide transfer activity was measured in triplicate for each protein.

Immunofluorescence Microscopy of CERT Cellular Localization
An HA-epitope tag was added to the N-terminus of CERT and CERT E494R/N495K/P535R/E537K by PCR. HEK293 cells were transfected with either HA-CERT or HA-CERT-E494R/N495K/P535R/E537K in pcDNA6/V5-His expression plasmids by calcium phosphate precipitation. After 24 h, the transfected cells were fixed with 4% paraformaldehyde for 20 minutes, permeabilized with 0.2% Triton X-100 in PBS for 20 minutes, and then incubated in BlockAid™ Blocking Solution (Molecuar Probes) for 1 h at room temperature. The cells were then incubated with primary antibodies, rat anti-HA and mouse anti-GM130 (Golgi marker) or control IgG, diluted in PBS at 4 °C overnight. The cells

were briefly rinsed with PBS then incubated with secondary antibodies, anti-rat IgG labeled with Alexa Fluor® 488 and anti-mouse IgG labeled with Alexa Fluor® 594 for 1 h at room temperature. After intensive washing with PBS, the slides were mounted by cold Vectashield Hard Set mounting medium and visualized by an Olympus Fluoview 300 confocal microscope. The images were acquired with the PlanApo 100x objective using the Olympus FluoView 5.0 software. Images for Fig. 7 were prepared with ImageJ (45).

ACKNOWLEDGEMENTS
We thank Dr. Dominika Borek for help with X-ray crystallography, Dr. Andrew Keightley for help with mass spectrometry, Linda Feng and Dr. John Laity for help with ITC and NMR experiments, Drs. Thomas Scheuermann and Chad Brautigam for help with ITC data analysis. We also thank Drs. Jin-Yuan Price, Margaret Kincaid, and Christopher Nauman for help with fluorescence imaging. The x-ray diffraction data were collected at the Advanced Photon Source at the Argonne National Lab through the SER-CAT consortium.

CONFLICT OF INTEREST
The authors declare that they have no conflicts of interest with the contents of this article.

AUTHOR CONTRIBUTIONS
XY and JP designed the experiments and wrote the manuscript; JP either performed or participated in all the experiments; SB participated in crystal structure determination and edited the manuscript; MF, LY, and XY carried out the immunofluorescence microscopy experiments; DB carried out the HPA-12 synthesis.

REFERENCES

1. van Meer, G., and Holthuis, J. C. (2000) Sphingolipid transport in eukaryotic cells. *Biochim Biophys Acta* **1486**, 145-170
2. Hannun, Y. A., and Obeid, L. M. (2008) Principles of bioactive lipid signalling: lessons from sphingolipids. *Nat Rev Mol Cell Biol* **9**, 139-150
3. van Meer, G., and Sprong, H. (2004) Membrane lipids and vesicular traffic. *Curr Opin Cell Biol* **16**, 373-378
4. Giussani, P., Colleoni, T., Brioschi, L., Bassi, R., Hanada, K., Tettamanti, G., Riboni, L., and Viani, P. (2008) Ceramide traffic in C6 glioma cells: evidence for CERT-dependent and independent transport from ER to the Golgi apparatus. *Biochim Biophys Acta* **1781**, 40-51
5. Hanada, K., Kumagai, K., Yasuda, S., Miura, Y., Kawano, M., Fukasawa, M., and Nishijima, M. (2003) Molecular machinery for non-vesicular trafficking of ceramide. *Nature* **426**, 803-809
6. Yamaji, T., Kumagai, K., Tomishige, N., and Hanada, K. (2008) Two sphingolipid transfer proteins, CERT and FAPP2: their roles in sphingolipid metabolism. *IUBMB Life* **60**, 511-518
7. Sugiki, T., Takeuchi, K., Yamaji, T., Takano, T., Tokunaga, Y., Kumagai, K., Hanada, K., Takahashi, H., and Shimada, I. (2012) Structural basis for the Golgi association by the pleckstrin homology domain of the ceramide trafficking protein (CERT). *J Biol Chem* **287**, 33706-33718
8. Prashek, J., Truong, T., and Yao, X. (2013) Crystal structure of the pleckstrin homology domain from the ceramide transfer protein: implications for conformational change upon ligand binding. *PLoS One* **8**, e79590
9. Kawano, M., Kumagai, K., Nishijima, M., and Hanada, K. (2006) Efficient trafficking of ceramide from the endoplasmic reticulum to the Golgi apparatus requires a VAMP-associated protein-interacting FFAT motif of CERT. *J Biol Chem* **281**, 30279-30288
10. Peretti, D., Dahan, N., Shimoni, E., Hirschberg, K., and Lev, S. (2008) Coordinated lipid transfer between the endoplasmic reticulum and the Golgi complex requires the VAP proteins and is essential for Golgi-mediated transport. *Mol Biol Cell* **19**, 3871-3884
11. Kumagai, K., Kawano-Kawada, M., and Hanada, K. (2014) Phosphoregulation of the ceramide transport protein CERT at serine 315 in the interaction with VAMP-associated protein (VAP) for inter-organelle trafficking of ceramide in mammalian cells. *J Biol Chem* **289**, 10748-10760
12. Kumagai, K., Kawano, M., Shinkai-Ouchi, F., Nishijima, M., and Hanada, K. (2007) Interorganelle trafficking of ceramide is regulated by phosphorylation-dependent cooperativity between the PH and START domains of CERT. *J Biol Chem* **282**, 17758-17766
13. Fugmann, T., Hausser, A., Schöffler, P., Schmid, S., Pfizenmaier, K., and Olayioye, M. A. (2007) Regulation of secretory transport by protein kinase D-mediated phosphorylation of the ceramide transfer protein. *J Cell Biol* **178**, 15-22
14. Tomishige, N., Kumagai, K., Kusuda, J., Nishijima, M., and Hanada, K. (2009) Casein kinase I{gamma}2 down-regulates trafficking of ceramide in the synthesis of sphingomyelin. *Mol Biol Cell* **20**, 348-357
15. Krissinel, E., and Henrick, K. (2007) Inference of macromolecular assemblies from crystalline state. *J Mol Biol* **372**, 774-797
16. Kudo, N., Kumagai, K., Matsubara, R., Kobayashi, S., Hanada, K., Wakatsuki, S., and Kato, R. (2010) Crystal structures of the CERT START domain with inhibitors provide insights into the mechanism of ceramide transfer. *J Mol Biol* **396**, 245-251
17. Tsujishita, Y., and Hurley, J. H. (2000) Structure and lipid transport mechanism of a StAR-related domain. *Nat Struct Biol* **7**, 408-414

18. Kudo, N., Kumagai, K., Tomishige, N., Yamaji, T., Wakatsuki, S., Nishijima, M., Hanada, K., and Kato, R. (2008) Structural basis for specific lipid recognition by CERT responsible for nonvesicular trafficking of ceramide. *Proc Natl Acad Sci U S A* **105**, 488-493
19. Lemmon, M. A. (2007) Pleckstrin homology (PH) domains and phosphoinositides. *Biochem Soc Symp*, 81-93
20. Winn, M. D., Ballard, C. C., Cowtan, K. D., Dodson, E. J., Emsley, P., Evans, P. R., Keegan, R. M., Krissinel, E. B., Leslie, A. G., McCoy, A., McNicholas, S. J., Murshudov, G. N., Pannu, N. S., Potterton, E. A., Powell, H. R., Read, R. J., Vagin, A., and Wilson, K. S. (2011) Overview of the CCP4 suite and current developments. *Acta Crystallogr D Biol Crystallogr* **67**, 235-242
21. Bielefeld-Sevigny, M. (2009) AlphaLISA immunoassay platform- the "no-wash" high-throughput alternative to ELISA. *Assay Drug Dev Technol* **7**, 90-92
22. Yasuda, S., Kitagawa, H., Ueno, M., Ishitani, H., Fukasawa, M., Nishijima, M., Kobayashi, S., and Hanada, K. (2001) A novel inhibitor of ceramide trafficking from the endoplasmic reticulum to the site of sphingomyelin synthesis. *J Biol Chem* **276**, 43994-44002
23. Nakamura, Y., Matsubara, R., Kitagawa, H., Kobayashi, S., Kumagai, K., Yasuda, S., and Hanada, K. (2003) Stereoselective synthesis and structure-activity relationship of novel ceramide trafficking inhibitors. (1R,3R)-N-(3-hydroxy-1-hydroxymethyl-3-phenylpropyl)dodecanamide and its analogues. *J Med Chem* **46**, 3688-3695
24. Ďuriš, A., Wiesenganger, T., Moravčíková, D., Baran, P., Kožíšek, J., Daïch, A., and Berkeš, D. (2011) Expedient and practical synthesis of CERT-dependent ceramide trafficking inhibitor HPA-12 and its analogues. *Org Lett* **13**, 1642-1645
25. Corbin, J. A., Dirkx, R. A., and Falke, J. J. (2004) GRP1 pleckstrin homology domain: activation parameters and novel search mechanism for rare target lipid. *Biochemistry* **43**, 16161-16173
26. Mattjus, P., Molotkovsky, J. G., Smaby, J. M., and Brown, R. E. (1999) A fluorescence resonance energy transfer approach for monitoring protein-mediated glycolipid transfer between vesicle membranes. *Anal Biochem* **268**, 297-304
27. Tuuf, J., Kjellberg, M. A., Molotkovsky, J. G., Hanada, K., and Mattjus, P. (2011) The intermembrane ceramide transport catalyzed by CERT is sensitive to the lipid environment. *Biochim Biophys Acta* **1808**, 229-235
28. Gronenborn, A. M., Filpula, D. R., Essig, N. Z., Achari, A., Whitlow, M., Wingfield, P. T., and Clore, G. M. (1991) A novel, highly stable fold of the immunoglobulin binding domain of streptococcal protein G. *Science* **253**, 657-661
29. Achari, A., Hale, S. P., Howard, A. J., Clore, G. M., Gronenborn, A. M., Hardman, K. D., and Whitlow, M. (1992) 1.67-A X-ray structure of the B2 immunoglobulin-binding domain of streptococcal protein G and comparison to the NMR structure of the B1 domain. *Biochemistry* **31**, 10449-10457
30. Gallagher, T., Alexander, P., Bryan, P., and Gilliland, G. L. (1994) Two crystal structures of the B1 immunoglobulin-binding domain of streptococcal protein G and comparison with NMR. *Biochemistry* **33**, 4721-4729
31. Saito, S., Matsui, H., Kawano, M., Kumagai, K., Tomishige, N., Hanada, K., Echigo, S., Tamura, S., and Kobayashi, T. (2008) Protein phosphatase 2Cepsilon is an endoplasmic reticulum integral membrane protein that dephosphorylates the ceramide transport protein CERT to enhance its association with organelle membranes. *J Biol Chem* **283**, 6584-6593
32. Otwinowski, Z., Minor, W., and Charles W. Carter, Jr. (1997) [20] Processing of X-ray diffraction data collected in oscillation mode. in *Methods in Enzymology*, Academic Press. pp 307-326
33. McCoy, A. J., Grosse-Kunstleve, R. W., Adams, P. D., Winn, M. D., Storoni, L. C., and Read, R. J. (2007) Phaser crystallographic software. *J Appl Crystallogr* **40**, 658-674

34. Afonine, P. V., Grosse-Kunstleve, R. W., Echols, N., Headd, J. J., Moriarty, N. W., Mustyakimov, M., Terwilliger, T. C., Urzhumtsev, A., Zwart, P. H., and Adams, P. D. (2012) Towards automated crystallographic structure refinement with phenix.refine. *Acta Crystallogr D Biol Crystallogr* **68**, 352-367
35. Murshudov, G. N., Vagin, A. A., and Dodson, E. J. (1997) Refinement of macromolecular structures by the maximum-likelihood method. *Acta Crystallogr D Biol Crystallogr* **53**, 240-255
36. Adams, P. D., Afonine, P. V., Bunkóczi, G., Chen, V. B., Davis, I. W., Echols, N., Headd, J. J., Hung, L. W., Kapral, G. J., Grosse-Kunstleve, R. W., McCoy, A. J., Moriarty, N. W., Oeffner, R., Read, R. J., Richardson, D. C., Richardson, J. S., Terwilliger, T. C., and Zwart, P. H. (2010) PHENIX: a comprehensive Python-based system for macromolecular structure solution. *Acta Crystallogr D Biol Crystallogr* **66**, 213-221
37. Emsley, P., Lohkamp, B., Scott, W. G., and Cowtan, K. (2010) Features and development of Coot. *Acta Crystallogr D Biol Crystallogr* **66**, 486-501
38. Chen, V. B., Arendall, W. B., Headd, J. J., Keedy, D. A., Immormino, R. M., Kapral, G. J., Murray, L. W., Richardson, J. S., and Richardson, D. C. (2010) MolProbity: all-atom structure validation for macromolecular crystallography. *Acta Crystallogr D Biol Crystallogr* **66**, 12-21
39. WL, D. (2002) The PyMOL Molecular Graphic System. http://www.pymol.org.http://www.pymol.org.
40. Keller, S., Vargas, C., Zhao, H., Piszczek, G., Brautigam, C. A., and Schuck, P. (2012) High-precision isothermal titration calorimetry with automated peak-shape analysis. *Anal Chem* **84**, 5066-5073
41. Scheuermann, T. H., and Brautigam, C. A. (2015) High-precision, automated integration of multiple isothermal titration calorimetric thermograms: new features of NITPIC. *Methods* **76**, 87-98
42. Houtman, J. C., Brown, P. H., Bowden, B., Yamaguchi, H., Appella, E., Samelson, L. E., and Schuck, P. (2007) Studying multisite binary and ternary protein interactions by global analysis of isothermal titration calorimetry data in SEDPHAT: application to adaptor protein complexes in cell signaling. *Protein Sci* **16**, 30-42
43. Brautigam, C. A., Deka, R. K., Schuck, P., Tomchick, D. R., and Norgard, M. V. (2012) Structural and thermodynamic characterization of the interaction between two periplasmic Treponema pallidum lipoproteins that are components of a TPR-protein-associated TRAP transporter (TPAT). *J Mol Biol* **420**, 70-86
44. Brautigam, C. A. (2015) Calculations and Publication-Quality Illustrations for Analytical Ultracentrifugation Data. *Methods Enzymol* **562**, 109-133
45. Schneider, C. A., Rasband, W. S., and Eliceiri, K. W. (2012) NIH Image to ImageJ: 25 years of image analysis. *Nature Methods* **9**, 671-675
46. Holst, M., Numerical Computing Group, D. o. C. S., University of Illinois at Urbana-Champaign, 1304 W. Springfield Ave., Urbana, Illinois 61801, Numerical Computing Group, D. o. C. S., University of Illinois at Urbana-Champaign, 1304 W. Springfield Ave., Urbana, Illinois 61801, Saied, F., and Numerical Computing Group, D. o. C. S., University of Illinois at Urbana-Champaign, 1304 W. Springfield Ave., Urbana, Illinois 61801. (1993) Multigrid solution of the Poisson—Boltzmann equation. *Journal of Computational Chemistry* **14**, 105-113
47. Holst, M. J., Department of Applied Mathematics and CRPC, C. I. o. T., Pasadena, California 91125, Department of Applied Mathematics and CRPC, C. I. o. T., Pasadena, California 91125, Saied, F., and Department of Computer Science, U. o. I. a. U. C., 1304 West Springfield Ave., Urbana, Illinois 61801. (1995) Numerical solution of the nonlinear Poisson–Boltzmann equation: Developing more robust and efficient methods. *Journal of Computational Chemistry* **16**, 337-364

48. Baker, N. A., Sept, D., Joseph, S., Holst, M. J., and McCammon, J. A. (2001) Electrostatics of nanosystems: application to microtubules and the ribosome. *Proc Natl Acad Sci U S A* **98**, 10037-10041
49. Bank, R. E., and Holst, M. (2003) A New Paradigm for Parallel Adaptive Meshing Algorithms. *SIAM Review* **22**, 1411-1443

TABLE 1. **Crystallographic data collection and refinement statistics**

Data collection[a]	
Space group	$P2_12_12_1$
Unit cell dimensions	
a, b, c (Å)	59.761 60.914 95.804
α, β, γ (º)	90, 90, 90
Wavelength (Å)	1.000
Resolution (Å)	38.97 (2.40)
Completeness (%)	97.8 (84.7)
Unique reflections	13856
Redundancy (fold)	12.3 (6.4)
$\langle I \rangle / \langle \sigma I \rangle$	19.9 (2.27)
R_{merge} (%)	12.5 (55.9)
Refinement	
Number of molecules/a.u.	2
R_{work}/R_{free} (%)	20.1/24.5
Number of non-hydrogen atoms	
Protein	2707
Ligand	31
Ramachandran plot (%)	
Favored	98
Allowed	1.5
Outliers	0.31
RMSD	
Bond lengths (Å)	0.003
Bond angles (º)	0.483
Average B-factor ($Å^2$)	46.19

[a]: Numbers in parentheses are for the highest-resolution shell.

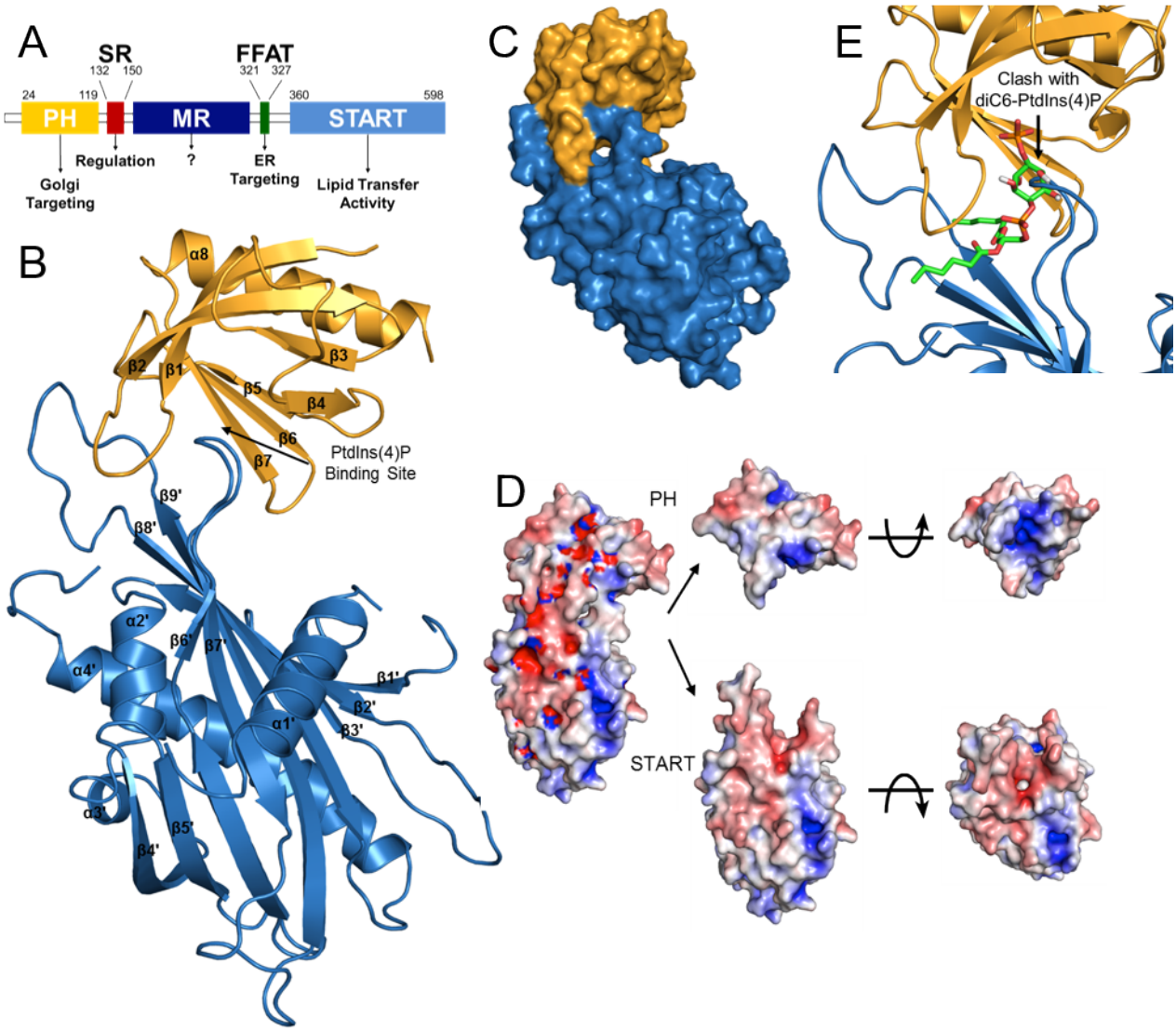

FIGURE 1. **Crystal structure of CERT PH and START complex at 2.4 Å resolution.** *A*, CERT domains and motifs. *B*, cartoon representation of the PH/START complex with PtdIns(4)P-binding site indicated (PDB code 5JJD; PH domain in *gold*, START domain in *blue*). *C,* surface representation of the PH/START complex. *D*, electrostatic surface potential of the PH/START complex (*left*) and its opened-up subunits (*right*) are colored at ±5kT/e (*red*, negative; *blue*, positive). The charge potential was calculated using APBS (46-49). *E*, superposition of the PH/START complex with a HADDOCK model of diC6-PtdIns(4)P (shown as stick model) docked onto CERT PH domain (PDB code 4HHV).

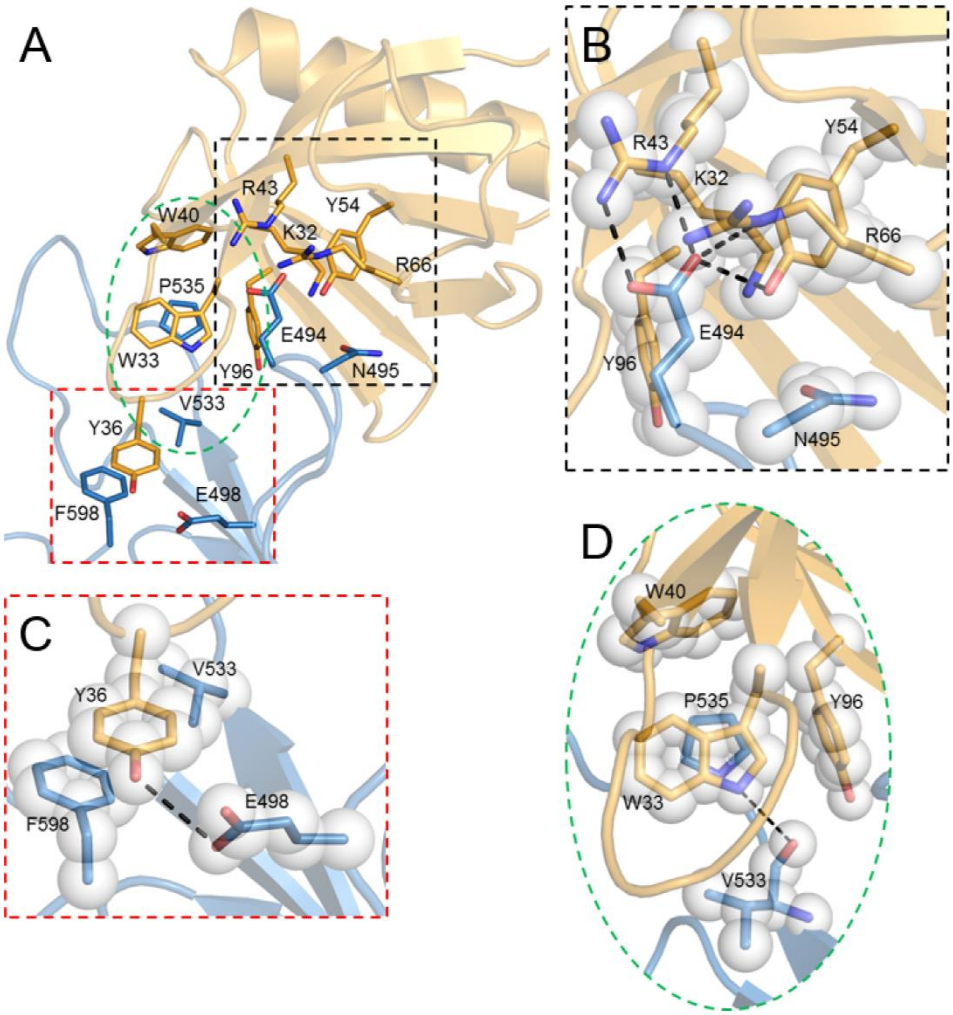

FIGURE 2. **Detailed interactions at the CERT PH/START interface.** *A*, residues involved in PH/START complex formation are shown as stick models (PDB code 5JJD; PH domain in *gold*, START domain in *blue*). *B*, key interactions between the PH domain and the β6'/β7' loop of the START domain. Potential hydrogen bonds are shown as *black dashed lines.* Translucent spheres are used to indicate van der Waals contacts. *C*, interactions between Tyr^{36} of the PH domain and Phe^{598} and Glu^{498} of the START domain. *D*, key interactions between the PH domain and the β8'/β9' loop of START domain. Potential salt bridges shown as *green dashed lines*.

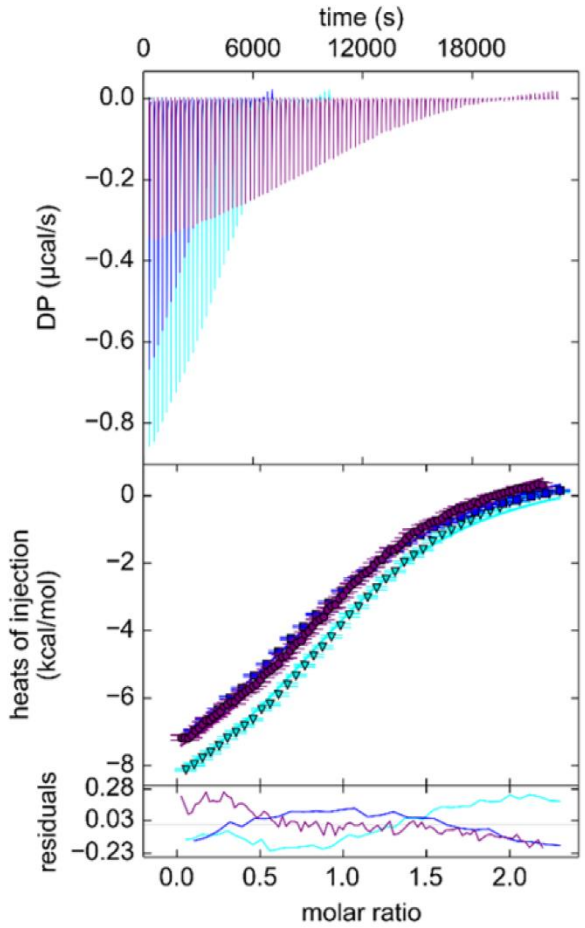

K_D (µM)	ΔH (kcal/mol)	Inc Fraction
9.2 (8.1, 10.5)	-12.1 (-13.1, -11.3)	0.08 (syringe)

FIGURE 3. **Binding affinity between CERT PH and START domains measured by ITC**. Global fitting of three independent ITC experiments. The best-fit values for K_D and ΔH are reported followed by the 1σ error intervals in parentheses. The incompetent (Inc) fraction reflects the difference between the stated concentration of PH domain and the concentration of binding competent material that best fits the data.

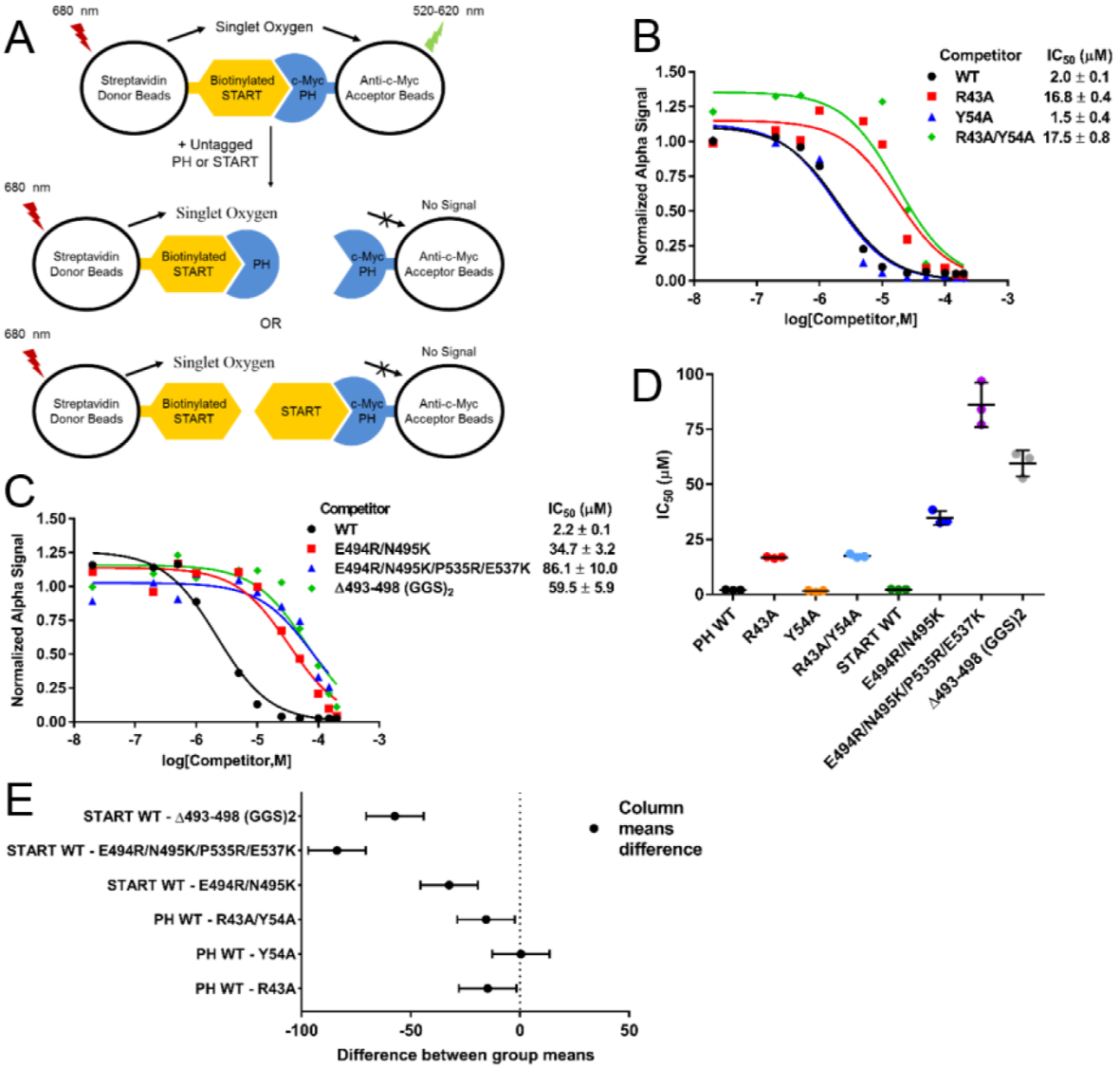

FIGURE 4. **CERT START domain β6'/β7' and β8'/β9' loops interact with PH through its PtdIns(4)P-binding site.** The PH/START interface was evaluated by an AlphaScreen competition assay. *A,* design of the AlphaScreen competition assay. Biotinylated START and c-Myc PH domain are immobilized on streptavidin coated donor beads and anti-c-Myc coated acceptor beads, respectively. Illumination of donor beads produces singlet oxygen. Interaction between the tagged PH and START domains brings donor and acceptor beads into close proximity allowing energy from singlet oxygen to be transferred to the acceptor beads and produce a light signal. Addition of untagged competitor proteins reduces the signal. *B,* competition for binding to biotinylated START domain by untagged PH WT and PH domain mutants. *C,* competition for binding to c-Myc PH domain by untagged START WT and START domain mutants. Each competitor was tested in duplicate or triplicate with a representative data set shown. Data analysis and curve fitting parameters are found under "Experimental Procedures". Legends for panels *B* and *C* are *inset*. *D*, The mean and standard deviations for the IC_{50} values measured in *B* and *C*. *E*, one-way ANOVA analysis of the IC_{50} values measured in *B* and *C*. Shown are the Sidak 99% confidence intervals for the Sidak's multiple comparisons tests.

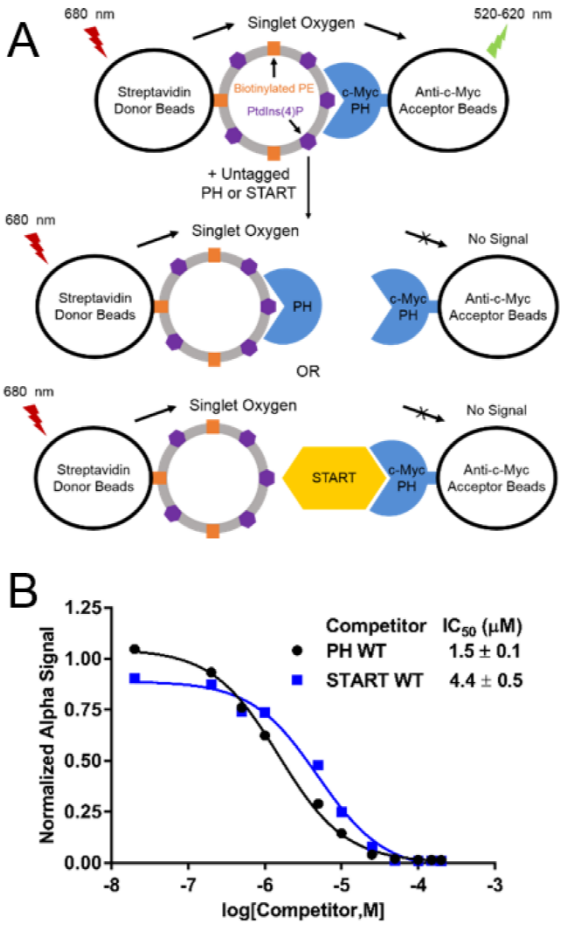

FIGURE 5. **CERT START domain competes with PtdIns(4)P for binding to the PH domain.** START domain competition with PtdIns(4)P for PH domain binding was evaluated by an AlphaScreen competition assay. *A,* design of the AlphaScreen competition assay. Same as in Fig. 4 except with liposomes containing biotinylated PE and PtdIns(4)P immobilized on streptavidin coated donor beads in place of the START domain. *B,* competition for binding to c-Myc PH domain by untagged PH or START domains. Each competitor was tested in triplicate with a representative data set shown. Data analysis and curve fitting parameters are found under "Experimental Procedures". Legend for panel *B* is *inset*.

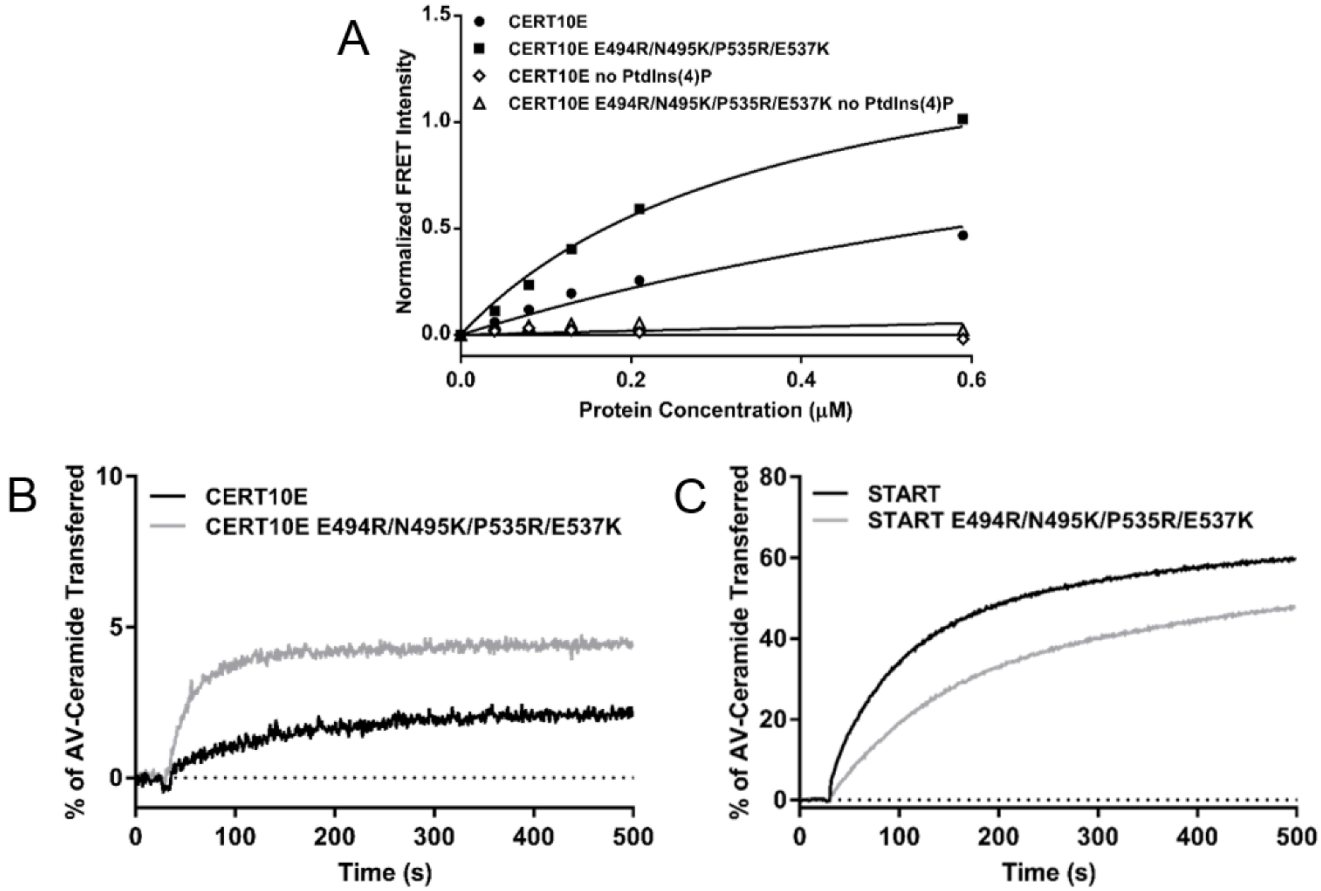

FIGURE 6. **Disruption of the PH/START interaction increases both PtdIns(4)P binding and ceramide transfer activity of a phosphorylation mimic CERT** *A*, binding of CERT10E and CERT10E E494R/N495K/P535R/E537K to liposomes detected by FRET between protein tryptophan residues and dansyl-PE lipids embedded in the liposomes. Shown is a representative plot of normalized FRET intensities at increasing protein concentrations with 40 μM liposomes containing 4mol% or no PtdIns(4)P. *B*, ceramide transfer activity of CERT proteins as monitored by the fluorescence emission of AV-Cer. Shown are representative runs of CERT10E and CERT10E E494R/N495K/P535R/E537K activity. *C*, representative runs measuring the ceramide transfer activity of START WT domain and START E494R/N495K/P535R/E537K. All activity assays were repeated in triplicate for each protein. Replicates are shown in Fig. S7. Legends are *inset*.

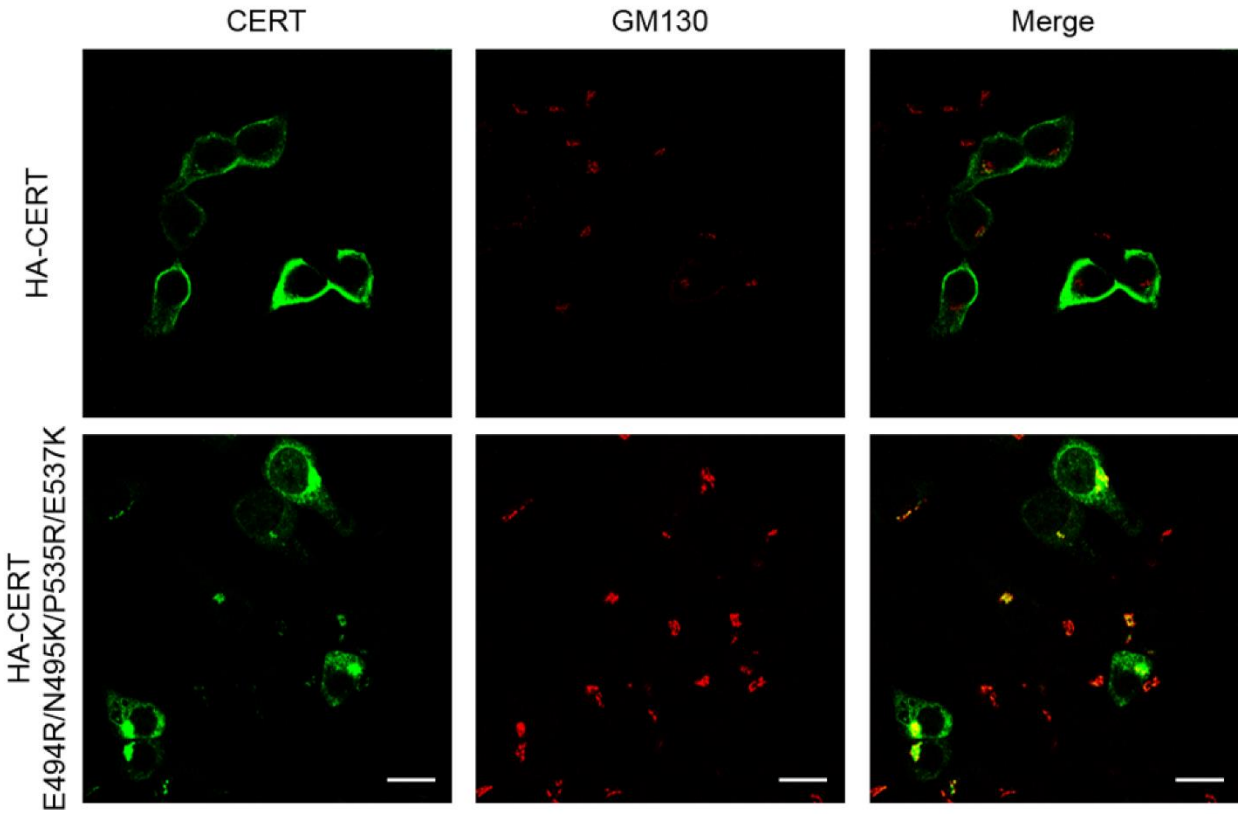

FIGURE 7. **Disruption of the PH/START interaction changes CERT cellular distribution.** HEK293 cells were transfected with plasmids encoding either HA-CERT (top row) or HA-CERT-E494R/N495K/P535R/E537K (bottom row). The transfectants were incubated with primary antibodies, rat anti-HA and mouse anti-GM130 (Golgi marker), then stained with secondary antibodies, anti-rat IgG labeled with Alexa Fluor® 488 (*green*) and anti-mouse IgG labeled with Alexa Fluor® 594 (*red*). Scale bars: 25 μM.

Interaction between the PH and START domains of ceramide transfer protein competes with phosphatidylinositol 4-phosphate binding by the PH domain

Jennifer Prashek, Samuel Bouyain, Mingui Fu, Yong Li, Dusan Berkes and Xiaolan Yao

J. Biol. Chem. published online June 26, 2017